Progress In Electromagnetics Research, PIER 74, 217–240, 2007

ANALYSIS OF PLANAR DIELECTRIC MULTILAYERS AS FSS BY TRANSMISSION LINE TRANSFER MATRIX METHOD (TLTMM)

H. Oraizi and M. Afsahi

Department of Electrical Engineering,
Iran University of Science and Technology
Narmak, 16844 Tehran, Iran

Abstract—The transmission line transfer matrix method (TLTMM) is presented for the analysis of multilayer electric structures as frequency selective surfaces (FSS), whereby the reflection, transmission and absorption coefficients, field distribution and power flow may be computed inside and outside of the layers. The TLTMM formulation may be developed for any arbitrary angle of incidence, any polarization (linear TE or TM, circular, elliptical) of the incident plane wave, at any frequency of operation (microwave, millimeter wave, optical), any number dielectric layers with arbitrary thicknesses, lossless or low loss dielectric media, inclusion of dispersion relation, etc. A general formulation is given for both the TE and TM polarization of the incident wave. Several practical situations are treated by TLTMM namely, anti-reflection coatings, high reflection surfaces, computation of the axial ratio of the reflected and transmitted plane waves, distributed brag reflector (DBR), a narrow band filter consisting of two Fabry-Perot resonators, cantor superlattices in optics, field distribution and power flow for a multilayer structure. Consequently, it is verified that TLTMM is capable of analysis a variety of practical multilayer dielectric structures.

1. INTRODUCTION

Frequency selective surfaces (FSS) for microwave and optical systems are usually realized by printed circuit technology, whereby their frequency selective characteristics are determined by the shape and periodic spacing of conducting patches. Theoretical and experimental investigations on FSS were first conducted on dipoles, tripoles, crossed dipoles, rings and square loops [1] and then were concentrated on more

complex structures [2–4] in order to decrease the size of elements. Although, the metallic FSS works well in the microwave frequencies, their application in the millimeter wave (MMW) and optical frequency ranges suffer from increased power losses and limitations of conducting surface thickness.

Structures consisting of periodic dielectric rods with permittivities ε_1 and ε_2 have been proposed for FSS in MMW frequency ranges [5]. Although, such structures provide reasonable transmission bandwidths for incident TE waves, their reflection bandwidths are drastically narrow (less than 2.5%), which leads to their limited applications. Such limitations have been removed by multilayer dielectric structures [6, 7]. Multilayer dielectric structures not only increase the bandwidths, but also provide identical amplitude responses for both TE and TM incident waves. However, their phase responses for TE and TM waves are usually different which adversely affect the incident circularly and elliptically polarized waves.

Multilayer dielectric structures have a variety of applications in the microwave [8], MMW [9] and optical frequencies [10], such as Radom anti-reflection coverings, high reflection layers, analysis of signal scattering from underground layers for oil and other mineral explorations, thin film optical filters, edge filters, dielectric mirrors in Fabry-Perot lasers, optical polarizer and shielding in optical bands, etc. The main advantage of dielectric structures compared with metallic surfaces is their less absorption losses in the MMW frequencies. However, in order to decrease losses, weight and volume of FSS structures, the number of layers in the microwave, and MMW frequencies should be limited.

Dielectric structures such as FSS have been introduced in the literature [5–7, 11–14] and have been analyzed by different methods. The multilayer dielectric FSS structures were first introduced in [6, 7] and were analyzed by the ABCD matrix method, and also in [15]. The ABCD matrix method calculates the reflection and transmission coefficients. They were also analyzed by a full-wave propagation method leading to a closed-form solution [16] that has also been used for the multilayer metamaterial structures [17]. In the full-wave method, the boundary conditions on two consecutive boundary surfaces are invoked to obtain a relation between the fields on them. Accordingly, a recursive relation is obtained to compute the reflection and transmission coefficients. In a matrix method [18, 19] the boundary conditions are invoked simultaneously at all boundaries, and the resulting matrix equation is solved for the reflection and transmission coefficients. In the iterative method [20], in each iteration a layer of the structure is removed and its effect on the reflection and transmission

coefficients is considered at the surface of structure. This process is continued until the overall coefficients of structure are calculated. The iterative method is also used for the metamaterial multilayer structures [21]. In the transfer matrix method (TMM) [22], the whole structure is divided into smaller elements and the system transfer matrix is obtained by using the properties of ABCD matrices. Consequently, the outgoing wave from the structure is computed from the incident wave by the transfer matrix. The transfer matrix method has been used for the calculation of reflection and transmission coefficients due to optical filters and metallic photonic band gaps (PBG). In the transmission line method [23], the reflection coefficient at the surface of the first layer is obtained by starting the calculations from the last layer using the impedance matching concept.

In this paper, we present a general formulation for the analysis of multilayer dielectric layers namely Transmission Line Transfer Matrix Method (TLTMM) combining the transmission line model and transfer matrix method. This formulation is equally applicable for both TE and TM incident wave polarizations. Consequently, the computer simulation of both cases may be combined so that the general elliptical polarization of the incident wave (including the circular polarization) may be readily treated by the proposed method. The field solutions are obtained in the inside and outside of layers.

2. FORMULATION OF THE PROBLEM

Consider an isotropic and homogeneous multilayer medium with boundary surfaces at $z = d_1, d_2, ..., d_N$ as shown in Fig. 1.

Each layer is homogeneous with electric and magnetic constants ε_ℓ, μ_ℓ, σ_ℓ. The 0'th and (N+1)'th media are half spaces which may have different characteristics. A plane wave is incident at an angle θ_0 on the multilayer structure from the 0'th medium. The plane of incidence is parallel with the y-z plane. The field components depend on y and z but are independent of x (i.e. $\partial/\partial x = 0$). The fields in each layer are decomposed into TE and TM polarization plane waves, and are expressed in terms of field components $E_{\ell x}$ and $H_{\ell x}$, respectively.

For the TE plane wave, the incident electric field is denoted as $\overrightarrow{E_i} = \widehat{x} E_0 e^{-(\gamma_y y + \gamma_z z)}$, and the other field components may be obtained from the Maxwell's equations as:

$$\left(\frac{\partial^2}{\partial y^2} + \frac{\partial^2}{\partial z^2} + \omega^2 \mu_\ell \varepsilon_\ell \right) E_{\ell x} = 0$$

$$H_{\ell y} = \frac{1}{j\omega\mu_\ell} \frac{\partial E_{\ell x}}{\partial z}$$

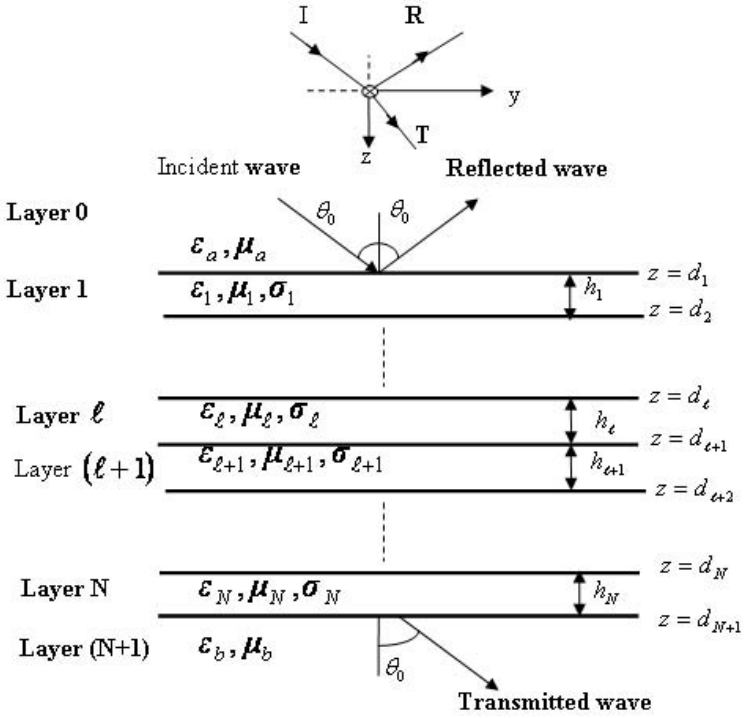

Figure 1. A multilayer dielectric structure as an FSS.

$$H_{\ell z} = \frac{-1}{j\omega\mu_\ell}\frac{\partial E_{\ell x}}{\partial y} \tag{1}$$

Consequently,

$$\begin{aligned} E_{\ell x} &= (E_\ell^+ e^{-\gamma_{\ell z} z} + E_\ell^- e^{+\gamma_{\ell z} z}) e^{-\gamma_{\ell y} y} \\ H_{\ell y} &= -\frac{\gamma_{\ell z}}{j\omega\mu_\ell}(E_\ell^+ e^{-\gamma_{\ell z} z} - E_\ell^- e^{+\gamma_{\ell z} z}) e^{-\gamma_{\ell y} y} \\ H_{\ell z} &= -\frac{\gamma_{\ell y}}{j\omega\mu_\ell}(E_\ell^+ e^{-\gamma_{\ell z} z} + E_\ell^- e^{+\gamma_{\ell z} z}) e^{-\gamma_{\ell y} y} \end{aligned} \tag{2}$$

For the TM plane wave, the incident magnetic field is denoted as $\overrightarrow{H_i} = \hat{x} H_0 e^{-(\gamma_y y + \gamma_z z)}$, and the other field components may be obtained from the Maxwell's equations or they may be obtained by duality using the replacements $\varepsilon_\ell \to \mu_\ell$, $\overrightarrow{E_\ell} \to \overrightarrow{H_\ell}$, $\overrightarrow{H_\ell} \to -\overrightarrow{E_\ell}$, in Eq. (1).

The boundary conditions on the tangential electric and magnetic field components on the boundary surfaces require the imposition of

phase matching. However for low loss media assumed here, the factors $e^{-\gamma_{\ell y} y}$ may be combined with coefficients $E_\ell^{\pm}$ and are not consider explicitly. Therefore the transverse field components Eq. (2) and their duality may be written for a constant y as:

for a TE plane wave

$$\begin{aligned} E_{\ell x} &= (E_\ell^+ e^{-\gamma_{\ell z} z} + E_\ell^- e^{+\gamma_{\ell z} z}) \\ H_{\ell y} &= -\frac{1}{Z_{0\ell}^{TE}}(E_\ell^+ e^{-\gamma_{\ell z} z} - E_\ell^- e^{+\gamma_{\ell z} z}) \end{aligned} \tag{3}$$

and for a TM plane wave

$$\begin{aligned} H_{\ell x} &= (H_\ell^+ e^{-\gamma_{\ell z} z} + H_\ell^- e^{+\gamma_{\ell z} z}) \\ E_{\ell y} &= Z_{0\ell}^{TM}(H_\ell^+ e^{-\gamma_{\ell z} z} - H_\ell^- e^{+\gamma_{\ell z} z}) \end{aligned} \tag{4}$$

Now, due to the resemblance of Eq. (1) and its dual to the transmission line relations, we may model the ℓ'th layer by a section of transmission line with propagation constant $\gamma_{\ell z}$ (which is the same for both TE and TM polarizations)

$$\begin{aligned} \gamma_{\ell z} &= \gamma_\ell \cos\theta_\ell \\ \gamma_\ell &= j\omega\sqrt{\mu_\ell \varepsilon_\ell} \\ \varepsilon_\ell &= \varepsilon^{'} - j\left(\varepsilon'' + \frac{\sigma}{\omega}\right) \end{aligned} \tag{5}$$

and characteristic impedances $Z_{0\ell}^{TE}$ and $Z_{0\ell}^{TM}$ which are the same as the wave impedances for TE and TM plane waves, respectively, are

$$\begin{aligned} Z_{0\ell}^{TE} &= \frac{j\omega\mu_\ell}{\gamma_{\ell z}} = \eta_\ell \sec\theta_\ell \\ Z_{0\ell}^{TM} &= \frac{\gamma_{\ell z}}{j\omega\varepsilon_\ell} = \eta_\ell \cos\theta_\ell \end{aligned} \tag{6}$$

The intrinsic impedance of the ℓ'th layer is $\eta_\ell = \sqrt{\mu_\ell/\varepsilon_\ell}$ and the incident angle in the ℓ'th layer is θ_ℓ. The Snell's law between two adjacent layers ℓ and $(\ell+1)$ is

$$\gamma_\ell \sin\theta_\ell = \gamma_{(\ell+1)} \sin\theta_{(\ell+1)} \tag{7}$$

Consequently, the equivalent transmission line model in Fig. 2 will be analyzed for the plane wave oblique incidence on the multilayered medium in place of the multilayer structure in Fig. 1.

The voltages, currents, propagation constant, and characteristic impedances of the equivalent transmission line model are defined in

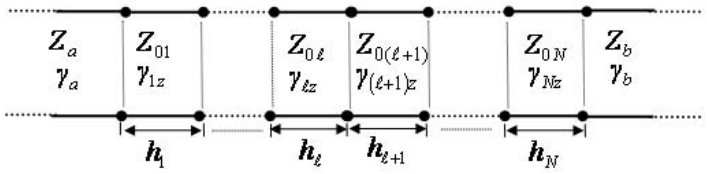

Figure 2. The equivalent transmission line circuit model for a multilayer dielectric structure.

Eqs. (3)–(6). In the equivalent transmission line model, the multiple reflected waves in the multilayered structure are combined as forward and backward traveling waves.

Now, we may define r and t as the total reflected and transmitted coefficients of structure, respectively, according to

$$r = \frac{E_0^-}{E_0^+} \qquad \text{in} \qquad \ell = 0 \tag{8}$$

$$t = \frac{E_{(N+1)}^+}{E_0^+} \qquad \text{in} \qquad \ell = N+1 \tag{9}$$

Also, we may define reflectance, transmittance and absorption as follows:

$$R = rr^* \tag{10}$$

$$T = tt^* \tag{11}$$

$$A = 1 - (R+T) \tag{12}$$

The wave amplitude transmission matrix of a layer and discontinuity transfer matrix may be defined with reference to Fig. 3 as:

$$\begin{bmatrix} E_{(\ell+1)}^+ \\ E_{(\ell+1)}^- \end{bmatrix} = [\,L\,]_{(\ell+1)} \begin{bmatrix} E_{(\ell+1)}^{\prime +} \\ E_{(\ell+1)}^{\prime -} \end{bmatrix} \tag{13}$$

$$\begin{bmatrix} E_{(\ell+1)}^{\prime +} \\ E_{(\ell+1)}^{\prime -} \end{bmatrix} = [\,I\,]_{(\ell+1)\ell} \begin{bmatrix} E_\ell^+ \\ E_\ell^- \end{bmatrix} \tag{14}$$

where $E^{\pm}$ and $E^{\prime \pm}$ are the forward and backward traveling waves at the end and beginning of each layer, respectively, $[L]_{(\ell+1)}$ is the wave amplitude transmission matrix of the $(\ell+1)$'th line section, and $[I]_{(\ell+1)\ell}$

is the transfer matrix of the discontinuity between the ℓ'th and $(\ell+1)$'th layer. Therefore

$$\begin{bmatrix} E^+_{(\ell+1)} \\ E^-_{(\ell+1)} \end{bmatrix} = [\,L\,]_{(\ell+1)}\,[\,L\,]_{(\ell+1)} \begin{bmatrix} E^+_{\ell} \\ E^-_{\ell} \end{bmatrix} \tag{15}$$

and the transfer matrix of a layer may be defined as:

$$[\,T\,]_{(\ell+1)\ell} = [\,L\,]_{(\ell+1)}\,[\,I\,]_{(\ell+1)\ell}\,, \qquad \ell = 0, 1, ..., N-1 \tag{16}$$

Consequently, the waves on the two outer sides of the multilayered medium between the 0'th and $(N+1)$'th layers are related as:

$$\begin{bmatrix} E^+_{(N+1)} \\ E^-_{(N+1)} \end{bmatrix} = [\,T\,]_{(N+1)0} \begin{bmatrix} E^+_{0} \\ E^-_{0} \end{bmatrix} \tag{17}$$

where

$$[\,T\,]_{(N+1)0} = [\,T\,]_{(N+1)N}\,[\,T\,]_{N(N-1)} \cdots [\,T\,]_{(\ell+1)\ell} \cdots [\,T\,]_{10} \tag{18}$$

Now, Eq. (17) is divided by E^+_0

$$\begin{bmatrix} t \\ 0 \end{bmatrix} = [\,T\,]_{(N+1)0} \begin{bmatrix} 1 \\ r \end{bmatrix} \tag{19}$$

which is expressed in terms of r and t according to the definitions of Eqs. (8) and (9). The outer half space is assumed matched ($E^-_{(N+1)} = 0$).

Consequently, r and t may be obtained from Eq. (19).

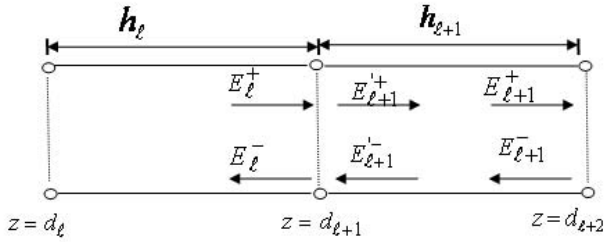

Figure 3. The forward and backward traveling waves inside two adjacent layer, where the wave is incident from ℓ'th layer onto $(\ell+1)$'th layer.

Referring to Fig. 3, matrix $[L]_{(\ell+1)}$ is

$$[L]_{(\ell+1)} = \begin{bmatrix} e^{-\gamma_{(\ell+1)z}h_{(\ell+1)}} & 0 \\ 0 & e^{\gamma_{(\ell+1)z}h_{(\ell+1)}} \end{bmatrix} \tag{20}$$

and matrix $[I]_{(\ell+1)\ell}$ is obtained for TE and TM polarizations, respectively.

For TE polarization, with reference to Fig. 3, we may write

$$\begin{aligned} E_\ell^- &= r_{(\ell+1)\ell}^{TE} E_\ell^+ + t_{\ell(\ell+1)}^{TE} E_{\ell+1}^{\prime -} \\ E_{\ell+1}^{\prime +} &= t_{(\ell+1)\ell}^{TE} E_\ell^+ + r_{\ell(\ell+1)}^{TE} E_{\ell+1}^{\prime -} \end{aligned} \tag{21}$$

where subscript x is deleted. $r_{(\ell+1)\ell}^{TE}$ and $t_{\ell(\ell+1)}^{TE}$ are the Fresnel reflection and transmission coefficients of the $\overrightarrow{E}$ field between the ℓ'th and $(\ell+1)$'th layers as [24]:

$$r_{(\ell+1)\ell}^{TE} = \frac{E_\ell^-}{E_\ell^+} = \frac{\eta_{(\ell+1)} \sec\theta_{(\ell+1)} - \eta_\ell \sec\theta_\ell}{\eta_{(\ell+1)} \sec\theta_{(\ell+1)} + \eta_\ell \sec\theta_\ell},$$

$$r_{\ell(\ell+1)}^{TE} = -r_{(\ell+1)\ell}^{TE} \tag{22}$$

$$t_{(\ell+1)\ell}^{TE} = \frac{E_{(\ell+1)}^+}{E_\ell^+} = 1 + r_{(\ell+1)\ell}^{TE} \tag{23}$$

Matrix $[I]_{(\ell+1)\ell}$ for TE polarization may be obtained by combining Eqs. (14), (21), (22) and (23).

$$[I]_{(\ell+1)\ell}^{TE} = \frac{1}{1 - r_{(\ell+1)\ell}^{TE}} \begin{bmatrix} 1 & -r_{(\ell+1)\ell}^{TE} \\ -r_{(\ell+1)\ell}^{TE} & 1 \end{bmatrix} \tag{24}$$

Similarly for TM polarization, we have

$$\begin{aligned} H_\ell^- &= r_{(\ell+1)\ell}^{TM} H_\ell^+ + t_{\ell(\ell+1)}^{TM} H_{\ell+1}^{\prime -} \\ H_{\ell+1}^{\prime +} &= t_{(\ell+1)\ell}^{TM} H_\ell^+ + r_{\ell(\ell+1)}^{TM} H_{\ell+1}^{\prime -} \end{aligned} \tag{25}$$

where subscript x is deleted. $r_{(\ell+1)\ell}^{TM}$ and $t_{(\ell+1)\ell}^{TM}$ are the Fresnel reflection and transmission coefficients of the $\overrightarrow{H}$ field between the ℓ'th and $(\ell+1)$'th layers. The reflection and transmission coefficients between two layers (for both TE and TM polarizations) are defined in terms of the electric field as [24]:

$$r_{(\ell+1)\ell}^{\prime TM} = \frac{E_{\ell y}^-}{E_{\ell y}^+} = \frac{\eta_{(\ell+1)} \cos\theta_{(\ell+1)} - \eta_\ell \cos\theta_\ell}{\eta_{(\ell+1)} \cos\theta_{(\ell+1)} + \eta_\ell \cos\theta_\ell},$$

$$r'^{TM}_{\ell(\ell+1)} = -r'^{TM}_{(\ell+1)\ell} \tag{26}$$

$$t'^{TM}_{(\ell+1)\ell} = \frac{E^+_{(\ell+1)y}}{E^+_{\ell y}} = (1 + r'^{TM}_{(\ell+1)\ell})\frac{\cos\theta_\ell}{\cos\theta_{(\ell+1)}} \tag{27}$$

The reflection and transmission coefficients with respect to the $\overrightarrow{H}$ field between two media may be related to those with respect to the $\overrightarrow{E}$ field according to the following relations:

$$r^{TM}_{(\ell+1)\ell} = \frac{H^-_{\ell x}}{H^+_{\ell x}} = \frac{\dfrac{-E^-_{\ell y}}{\eta_\ell}}{\dfrac{E^+_{\ell y}}{\eta_\ell}} = -\frac{E^-_{\ell y}}{E^+_{\ell y}} = -r'^{TM}_{(\ell+1)\ell} \tag{28}$$

$$\begin{aligned} t^{TM}_{(\ell+1)\ell} &= \frac{H^+_{(\ell+1)x}}{H^+_{\ell x}} = \frac{\dfrac{E^+_{(\ell+1)y}}{\eta_{(\ell+1)}}}{\dfrac{E^+_{\ell y}}{\eta_\ell}} = -\frac{E^-_{\ell y}}{E^+_{\ell y}} \\ &= (1 - r'^{TM}_{(\ell+1)\ell})\frac{\eta_\ell \cos\theta_\ell}{\eta_{(\ell+1)}\cos\theta_{(\ell+1)}} \end{aligned} \tag{29}$$

Equations (26) and (27) are substituted into Eqs. (28) and (29) and then in Eq. (25) to get

$$[I]^{TM}_{(\ell+1)\ell} = \frac{1}{(1 + r^{TM}_{(\ell+1)\ell})\dfrac{\eta_{(\ell+1)}\cos\theta_{(\ell+1)}}{\eta_\ell\cos\theta_\ell}} \begin{bmatrix} 1 & -r^{TM}_{(\ell+1)\ell} \\ -r^{TM}_{(\ell+1)\ell} & 1 \end{bmatrix} \tag{30}$$

Defining new variables

$$\begin{aligned} p^{TE}_{(\ell+1)\ell} &= \frac{\eta_{(\ell+1)}\sec\theta_{(\ell+1)}}{\eta_\ell \sec\theta_\ell}, \\ p^{TM}_{(\ell+1)\ell} &= \frac{\eta_\ell\cos\theta_\ell}{\eta_{(\ell+1)}\cos\theta_{(\ell+1)}} \end{aligned} \tag{31}$$

leads to the following unified notation for both TE and TM polarizations.

$$[I]^{TE/TM}_{(\ell+1)\ell} = \frac{1}{2}\begin{bmatrix} 1 + p^{TE/TM}_{(\ell+1)\ell} & 1 - p^{TE/TM}_{(\ell+1)\ell} \\ 1 - p^{TE/TM}_{(\ell+1)\ell} & 1 + p^{TE/TM}_{(\ell+1)\ell} \end{bmatrix} \tag{32}$$

Such formulation of the problem simplifies the computer simulation. Some observations are noteworthy.

First, since the incident plane coincides with the y-z plane, TE and TM polarizations have the field components (E_x, H_y, H_z) and (H_x, E_y, E_z) respectively, the forward and backward propagation powers may be computed by E_x for TE and H_x for TM polarizations.

Second, with reference to Fig. 1, Eq. (17) may be used to compute the forward and backward traveling waves in the ℓ'th layer $(\ell = 1, 2, ..., N)$ and then the reflection and transmission coefficients in each layer, according to the following relation:

$$\begin{bmatrix} E_\ell^+ \\ E_\ell^- \end{bmatrix} = [\,T\,]_{\ell(\ell+1)} \cdots [\,T\,]_{10} \begin{bmatrix} 1 \\ r \end{bmatrix} \tag{33}$$

Third, in case the medium in a layer is inhomogeneous, it may be subdivided into stepwise homogeneous layers with constants ε, μ, σ and then the proposed formulation may be applied.

Fourth, the incident wave with the general elliptical polarization (as a combination of TE and TM plane waves) may be treated and the reflected and transmitted waves from the multilayered medium are properly characterized.

3. NUMERICAL IMPLEMENTATION

The computer simulation of the proposed algorithm is performed according to the following flow chart using the aforementioned formulas. The computer input is the type of polarization of the incident wave (TE, TM, linear, circular, elliptical), angle of incidence (θ_i), operating frequency (f), number of layers (N), thicknesses of layers (H_ℓ), constants of each layer $(\varepsilon_{r\ell}, \mu_{r\ell}, \sigma_{r\ell}, \tan\delta_\ell)$, dispersion relations, etc. Then the transmission matrix $[L]_{(\ell+1)}$ of layers is computed by (20), variable $p^{TE/TM}$ and discontinuity transfer matrices $[I]_{(\ell+1)\ell}^{TM/TM}$ are computed by Eqs. (31) and (32), respectively. Now calculations proceed for the elliptic, circular, linear, TE and TM polarization, as the case may be. The transfer matrix $[T]_{(\ell+1)\ell}$ of each layer is computed by Eq. (16). Then, the overall transfer matrix $[T]_{(N+1)0}$ of the whole multilayer structure is computed by Eq. (18). The reflection and transmission coefficients (r, t) are computed by Eq. (19) and the reflectance, transmittance and absorption coefficients are computed by Eqs. (10), (11) and (12). The field and power variations may be plotted against frequency and angle of incidence.

4. EXAMPLES AND DISCUSSIONS

Several examples of oblique and normal incidence on different multilayered media are given below. There are N pairs of layers with high/low relative dielectric constants $\varepsilon_H/\varepsilon_L$. For example, $(HL)^N H$, indicates $2N + 1$ layers where the first layer has relative dielectric constant ε_H, the second one ε_L, etc.

4.1. Anti-reflection Coating

The quarter wavelength and half wavelength multilayer structures may be designed to make the reflection coefficient zero at a specified frequency and angle of incidence [24].

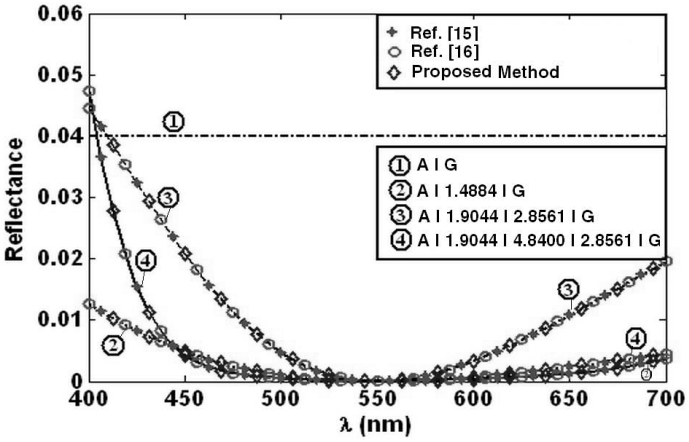

Figure 4. Frequency dependence of reflectance due to air-glass interface with and without coatings for reduction of reflection for visible light.

In order to achieve anti-reflection effect over a frequency bandwidth and range of incidence angles, a multilayered dielectric medium is required. In Fig. 4 reflectance is plotted against the wavelength for the following cases: air-glass $(A|G)$ without coating, $(A|1.4884|G)$ with a single quarter wavelength layer (with ε_r=1.4884), $(A|1.9044|2.8561|G)$ with two layers of quarter wavelength thickness (with ε_r=1.9044, ε_r=2.8561), and $(A|1.9044|4.8400|2.8561|G)$ with three layers with quarter-half-quarter wavelength thicknesses for normal incidence in the range of visible light (for glass ε_r=2.8). The results of the proposed method are compared with those of ABCD method [15] and full-wave propagation method [16]. It is observed

that the reflection from the double layer case is not better than that of the single layer case. However, addition of a half wavelength layer (with ε_r=4.84) has decreased reflection in the frequency range (450–700) nm. Reflection is a function of material and thickness of layers, frequency, angle of incidence and wave polarization. The reflection may be minimized or maximized with respect to the dielectric constant ($\varepsilon_{r\ell}$) and thickness of layers (h_ℓ) over a frequency bandwidth and incident angles.

4.2. High Reflection Coating

A multilayer dielectric medium with high reflection consists of an odd number of layers with periodic high/low permittivities of quarter wavelength thicknesses. The first layer has high ε_H. In optics, such a structure is called dielectric mirror or Bragg reflector.

In Fig. 5, the transmittance of a 21 layer high reflection structure with $(HL)^{10}H$ for TE and TM polarizations is plotted against frequency. It is located in air. The incidence angle is 0° and 40° and the frequency range is 100–300 GHz. The dielectric constants of layers are 5.0562 and 2.1025 and the thicknesses of the layers are equal to the quarter wavelength of the center frequency. The results are compared with the iterative method [20]. The transmittance depends on the angle of incidence. It becomes oscillatory and approaches zero out of the band. The transmittance characteristic is the same for both TE and TM polarizations.

4.3. Axial Ratio of Reflected and Transmitted Waves

The amplitude and phase responses of multilayer structures are different for waves with TE and TM polarizations, which causes the reflected and transmitted waves to become elliptically polarized for any linear, circular or elliptical polarization of the incident wave. Therefore, any incident wave may be decomposed into TE and TM polarized waves, and their behavior may be treated separately. Then they may be combined according to the superposition principle, to obtain the overall response. Fig. 6 shows the axial ratio of the dielectric structure with 9 layers $(LH)^4L$ with materials RT/Duroid 6010.5 ($\varepsilon_H = 10.5[1 - j0.0023]$) and RT/Duroid 5880 ($\varepsilon_L = 2.2[1 - j0.0009]$) for incident angles 20°, 25°, 30° at operating frequency 40 GHz. It is seem that in the indicated frequency range, with the decrease in the angle of incidence, the polarization of incident wave is maintained with little deviation. The axial ratio is calculated by Eq. (34) and is expressed in dB. The values of AR up to 6 dB, approximately denote

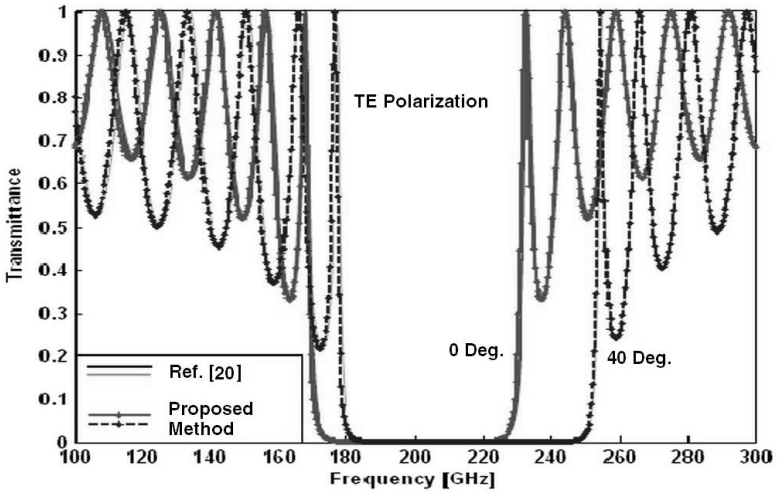

(a)

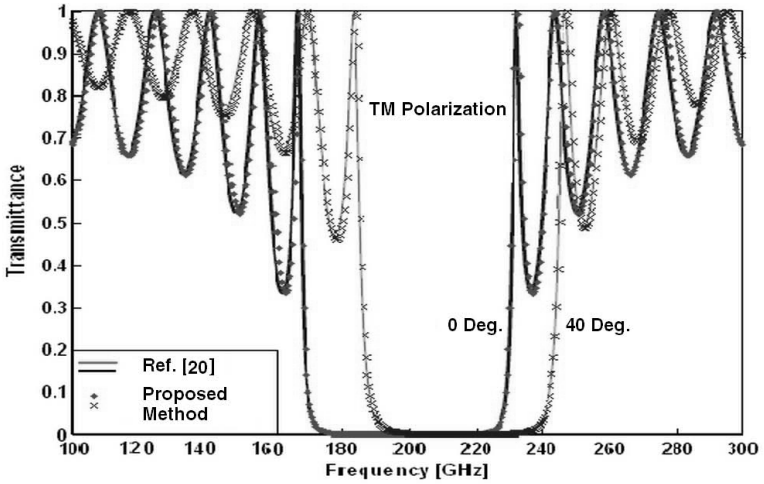

(b)

Figure 5. Frequency dependence of transmittance for a 21 dielectric layer FSS structure. The thickness of layers is equal to a quarter wavelength at $f_0 = 200\,\text{GHz}$. $\varepsilon_r = 5.0562$ for the first layer and 2.1025 and 5.00652 periodically for the succeeding layers; (a) TE polarization, (b) TM polarization.

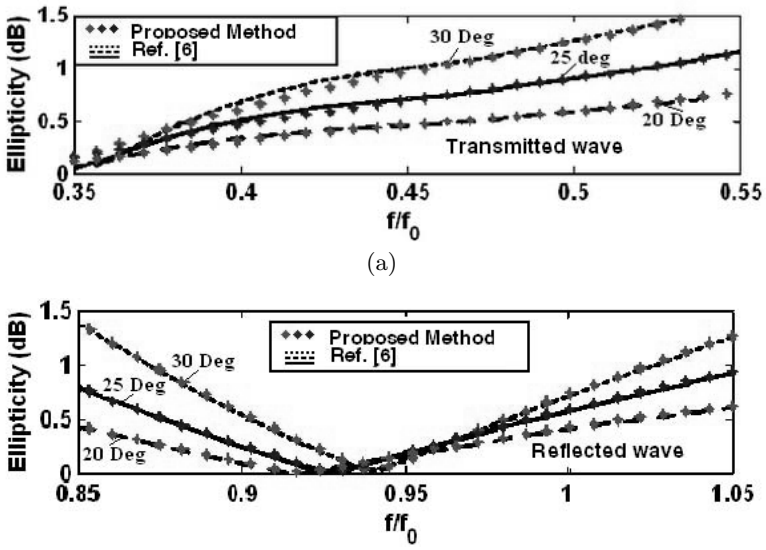

Figure 6. Axial ratio of the reflected and transmitted waves for a 9 layer FSS structure with the following specifications: $d_1 = d_9 = 3.139\,\text{mm}$, $d_2 = d_8 = 0.55\,\text{mm}$, $d_3 = d_7 = 1.269\,\text{mm}$, $d_4 = d_6 = 0.497\,\text{mm}$, $d_5 = 1.666\,\text{mm}$, $\varepsilon_{r(2\ell+1)} = 2.2$, $\varepsilon_{r(2\ell)} = 10.5$, $(n = 0, 1, ..., 4)$, $f_0 = 40\,\text{GHz}$; (a) transmitted wave axial ratio, (b) reflected wave axial ratio.

circular polarization.

$$AR = 20\log\left(\frac{E_{max}}{E_{min}}\right) \tag{34}$$

4.4. Distributed Bragg Reflector (DBR)

Distributed Bragg reflector consists of several pairs of layers, wherein each pair is made of different materials with different dielectric constants. DBR exhibits high reflection inside the Bragg regime which has applications in waveguides such as optical fibers.

Fig. 7 shows the reflectance of a high reflection structure consisting of 40 layers $(HL)^{20}$ as a DBR. The incident wave is normal at wavelength λ_0. The pair of layers is characterized by $\varepsilon_H = 4(1 - j0.001)$, $\mu_H = 1.02(1 - j0.001)$, ε_L=1 and $\mu_L = 1$. The thickness of a pair is p and that of the high ε_H is qp with $0 < q < 1$. Curves are

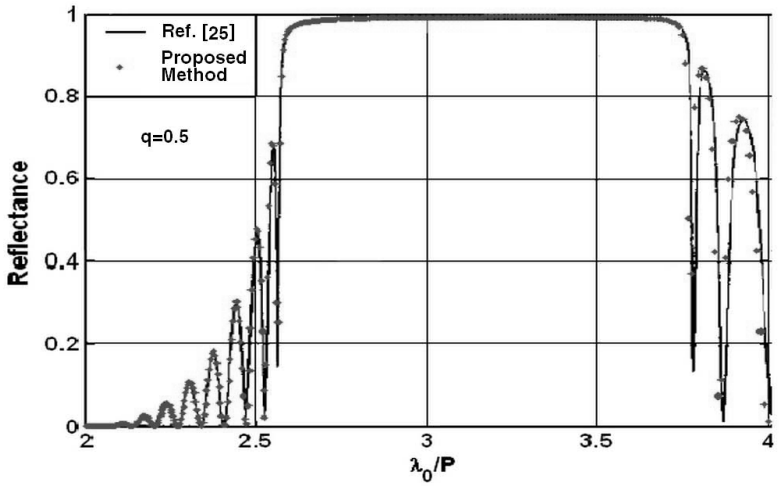

(a)

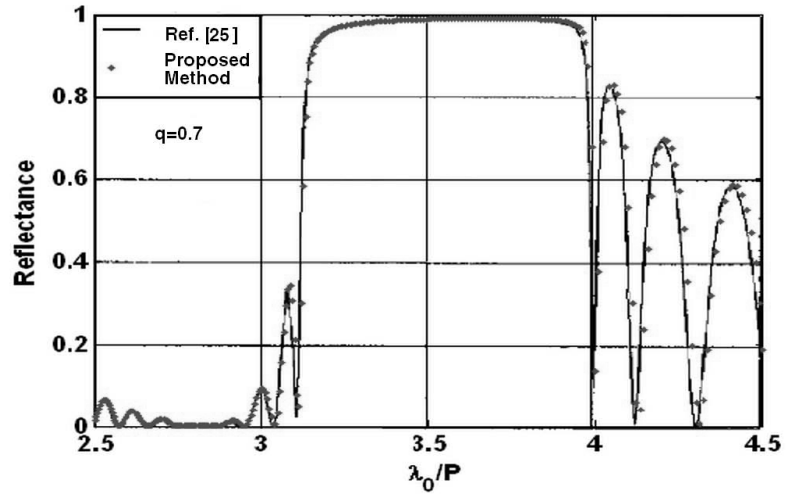

(b)

Figure 7. Reflectance of a 20 pair multilayer DBR with $\varepsilon_H = 4(1 - j0.001)$, $\mu_H = 1.02(1 - j0.001)$, $\varepsilon_L = 1$ and $\mu_L = 1$; (a) $q = 0.5$, (b) $q = 0.7$.

drawn in Fig. 7 for two values of $q = 0.5$ and $q = 0.7$. It is seen that as the value of q increases, the width of Bragg regime decreases and shifts towards the longer wavelength. The results agree well with Ref. [25].

4.5. A Narrow Band Filter Consisting of Two Fabry-Perot Resonators

Narrow band filters comprising of two Fabory-Perot filters are used in thin film technologies, fiber Bragg gratings, WDM multiplexers, narrow band laser sources ($\lambda_0 = 1550\,\text{nm}$), distributed feedback lasers, etc.

$(HL)^N$ structures make up a dielectric mirror which produces very high reflection coefficients. In such cases, H and L can have an arbitrary thickness, which is taken to be equal to a quarter wavelength here. The structure of $(HL)^N$L makes up a Fabry-Perot resonator (FPR). If the structure of $(HL)^N L(HL)^N L$ is sandwiched between identical substrates such as glass ($\varepsilon_r = 2.25$) in the form of $G|(HL)^N L(HL)^N L|G$, it will behave as a narrow band transfer filter at frequency λ_0. As N increases, the transfer range becomes narrower. An FPR with an odd number of layers with an extra layer of L at the end, such as $G|(HL)^{N1}L(HL)^{N1}|(HL)^{N2}L(HL)^{N2}|(HL)^{N3}L(HL)^{N3}L|G$ or an FPR with an even number of layers FPR without an extra layer of L, such as $G|(HL)^{N1}L(HL)^{N1}|(HL)^{N2}L(HL)^{N2}|G$ may be used for a narrow band transfer filter [26, 27].

Fig. 8 shows the transmittance for two types of FPR in the form of $G|(HL)^{N1}L(HL)^{N1}|(HL)^{N2}L(HL)^{N2}|G$ for two cases of $N_1 = N_2 = 8$ and $N_1 = N_2 = 9$. Layer thickness equal to a quarter wavelength at $\lambda_0 = 1550\,\text{nm}$ and normal incidence are considered. Fig. 8(a) shows the response in the range of wavelengths [1200–2000] nm for $N_1 = N_2 = 8$ and Fig. 8(b) shows it in [1549–1551] nm. It is seen that the transfer band is very narrow, and its bandwidth decrease as N increases.

4.6. Cantor Superlattice in Optics

Cantor superlattices have wide application in thin film transistors, laser technology, infrared photodetectors, etc.

Fig. 9 shows a cantor as pseudo periodic dielectric structure with a fractal dimension $\ln 2/\ln 3$ [28]. In this figure, the structure consists of two layers A and B with equal thicknesses ($d_A = d_{B1}$). The integer n indicates the order of generation, wherein the thickness of layer A is given by $d_{Bn} = 3^{n-1}d_{B1}$ and the number of layers is $N_n = 2N_{(n-1)} - 1$, $(n = 1, 2, ...)$. Here d_{B1} is the thickness of first layer and $N_0 = 1$.

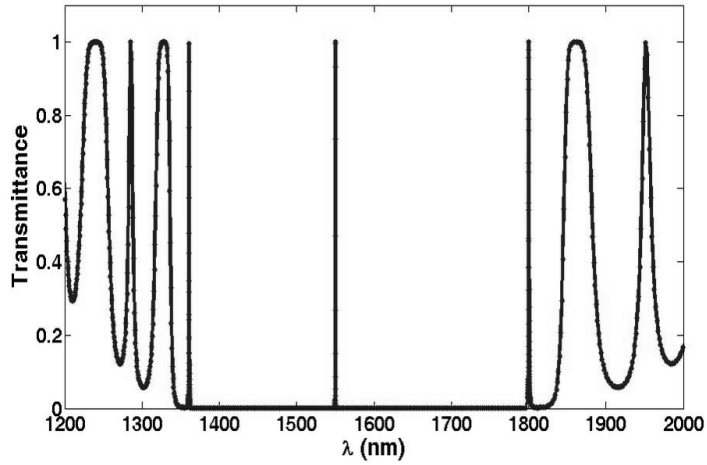

(a)

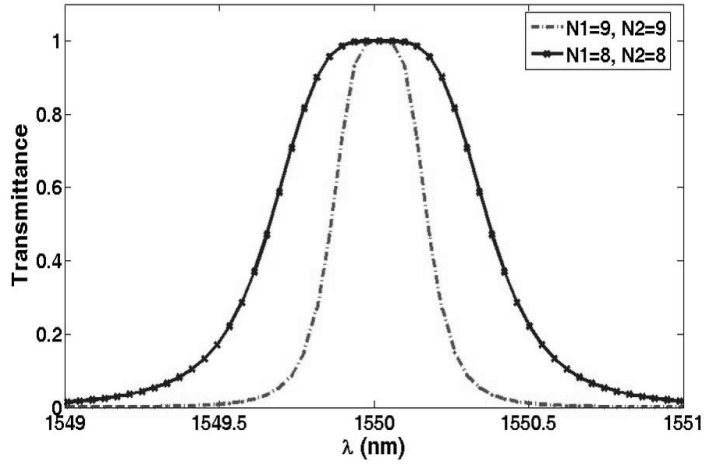

(b)

Figure 8. A narrow pass band filter composed of two FPR; (a) pass band filter characteristics in the [1200–2000] nm, (b) filter characteristics around $\lambda_0 = 1550\,\text{nm}$.

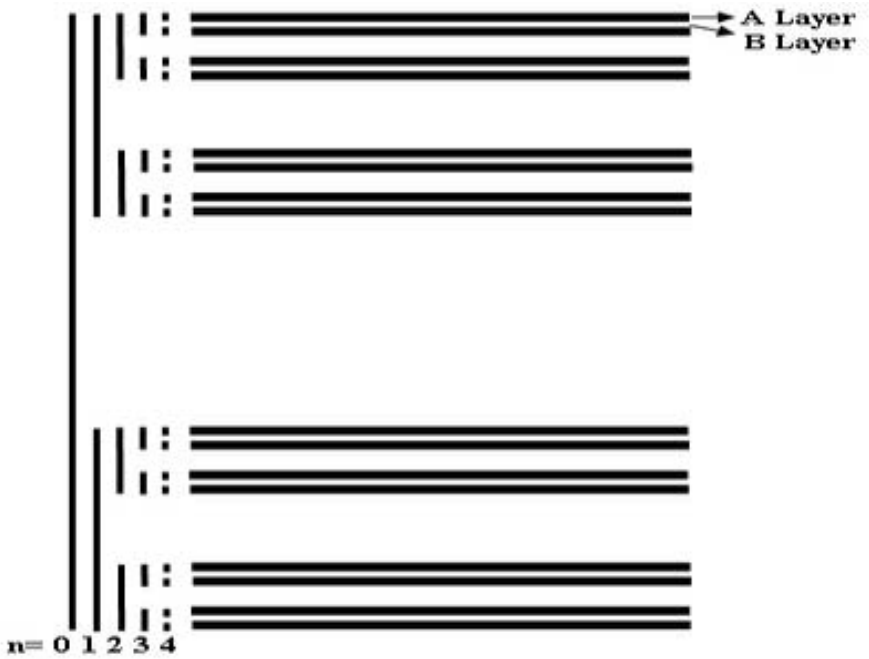

Figure 9. A pseudo periodic dielectric multilayer cantor superlattice with fractal dimension $\ln 2/\ln 3$.

Fig. 10 shows reflectance and transmittance of two cantors with 13 layers and $n = 3$, and 31 layers with $n = 4$. In this figure layers A and B are composed of $GaAs$ and SiO_2, respectively, with the following physical parameters: relative permittivity of layer B is assumed independent of frequency $\varepsilon_{rB} = 12.26$ and that of layer B is assumed to follow the plasma dispersion relation

$$\varepsilon_{rA}(\omega) = \varepsilon_{\infty A}(1 - \frac{\omega_{PA}^2}{\omega(\omega + j\Gamma_A)}) \tag{35}$$

where $\varepsilon_{\infty A} = 12.9$, and $\omega_{PA} = 4.04 \times 10^{12}$ Hz and $\Gamma_A = 0$ are the plasma angular frequency and attenuation constant, respectively. The thickness of layer A and B is equal to 40 nm, the incidence angle is 30° and the polarization is TM. The abscissa is the normalized frequency ω/Ω, with respect to

$$\Omega = \sqrt{\frac{n_A e^2}{m^* \varepsilon_0 \varepsilon_{\infty A} d_A}} = 2.294 \times 10^{13} \tag{36}$$

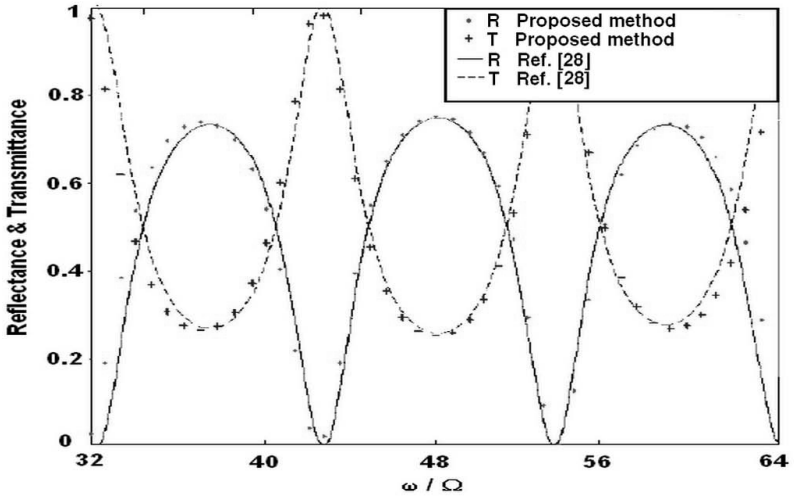

(a)

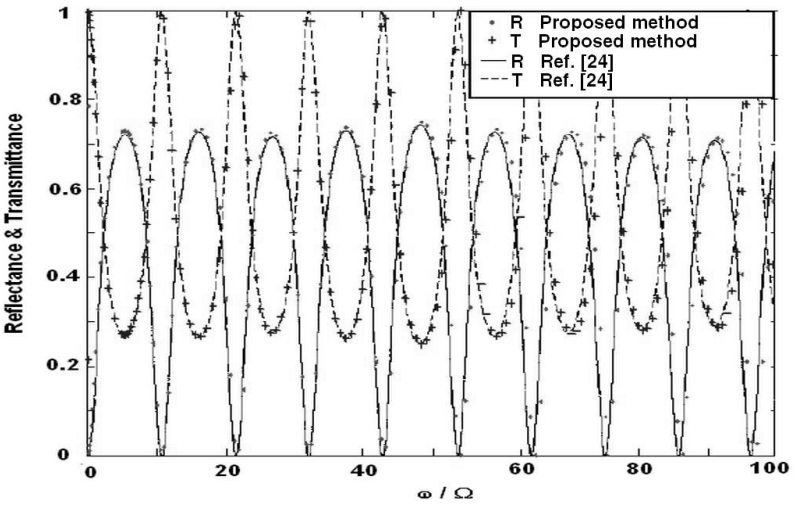

(b)

Figure 10. Frequency response of reflectance and transmittance of a cantor superlattice with the specification given in the text of paper; (a) third generation, (b) fourth generation.

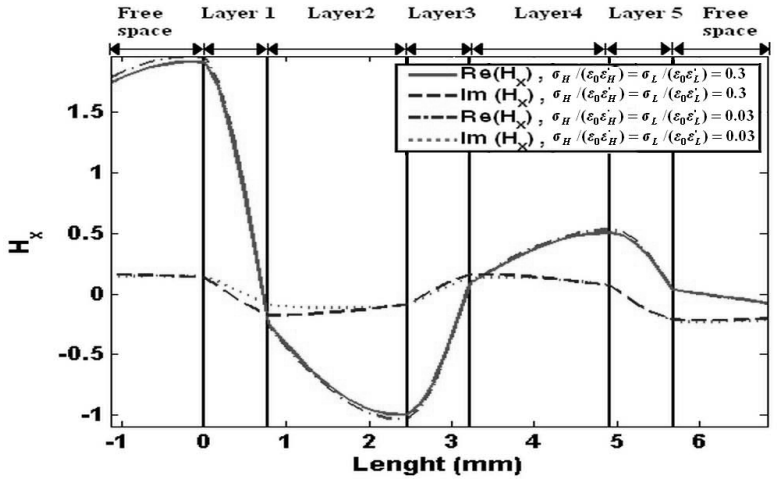

(a)

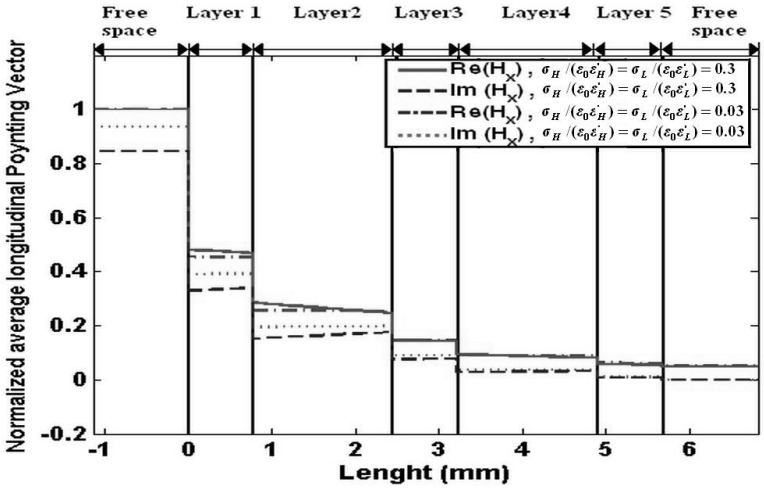

(b)

Figure 11. Forward and backward traveling fields and power in a 5 layer structure with TM polarization, angle of incidence 45°, frequency 30 GHz, $\varepsilon_r = 10.5(1 - j0.0023)$ for the first layer and $2.2(1 - j0.0009)$ and $10.5(1 - j0.0023)$ periodically for the succeeding layers and $\sigma_H/(\varepsilon_0\varepsilon'_H) = \sigma_L/(\varepsilon_0\varepsilon'_L) = 0.3, 0.03$ for all layers; (a) filed of H_x, (b) propagated power in z direction.

where carrier density is $n_A = 6 \times 10^{15}\,\mathrm{m}^{-2}$, $\mathrm{e} = 1.602 \times 10^{-19}\,\mathrm{C}$ and $m^* = 6.4 \times 10^{-32}\,\mathrm{Kg}$. Comparison of Figs. 10(a) and 10(b) shows that the increase of the generation order (n), the number of maxima increase and their frequency separations decrease. These results agree with those of [28].

4.7. Field Distribution and Forward and Backward Power Flow

Since the transmission line model is used for the multilayer dielectric structure, it is possible to obtain the field and also the forward and backward propagating powers insides the layers, as a function of position. Some of the other methods mentioned in the introduction do not possess such a capability, which may be considered as one of the advantages of the proposed method.

For example, Fig. 11(a) shows the real and imaginary parts of H_x field components and Fig. 11(b) shows the forward and backward propagating power in the direction for TM polarization inside and outside the layers. Fig. 11 is computed for the frequency 30 GHz, the normal incident, angle of incidence 45°, $\varepsilon_H = 10.5(1 - j0.0023)$, $\varepsilon_L = 2.2(1 - j0.0009)$, two cases of $\sigma_H/(\varepsilon_0\varepsilon'_H) = \sigma_L/(\varepsilon_0\varepsilon'_L) = 0.3, 0.03$ and a structure of 5 layers $(LH)^2L$ and layer thickness equal to a quarter wavelength. Continuity of the tangential magnetic field component H_x is evident in Fig. 11(a). It may be observed in Fig. 11(b) that due to the lossy nature of the layers, the propagating power in the z direction decreases. The incident, reflected, transmitted and dissipated powers in the layers are related by Eq. (12). The discontinuity in the power propagating in the z direction at the boundary between two adjacent layers is due to the change of direction of wave propagating in consecutive layers, which is obtained from Eq. (7). In Fig. 11(b), larger values of σ lead to high losses.

5. CONCLUSIONS

Multilayer dielectric structures behave as frequency selective surfaces (FSS) in front of incident waves. The frequency responses of reflected and transmitted waves due to such structures depend on frequency, angle of incidence, incident wave polarization, physical parameters of stratified media, and dispersion relation of materials. The proposed method namely Transmission Line Transfer Matrix Method (TLTMM) in this paper for their analysis uses the transmission line model, and the transfer matrix method and achieves exactly the same results obtained by several available methods. A unified formulation is derived for both

TE and TM polarizations, which facilitates the computer simulations. The generalized formulation may be used to treat any elliptically polarized incident wave. The field distribution and the propagating powers in the positive and negative z directions inside and outside layers may be readily computed and plotted. The proposed method is also capable of treating multilayer dielectric layer structure which are inhomogeneous in the direction normal to the layer faces. The TLTMM method may be used for multilayer metamaterial structure and also for obtaining optimum frequency selective structures.

REFERENCES

1. Mittra, R., C. H. Chan, and T. Cwik, "Techniques for analyzing frequency selective surfaces-a review," *Proceedings of the IEEE*, Vol. 76, No. 12, 1593–1615, 1988.
2. Parker, E. A. and A. N. A. El Sheikh, "Convoluted array elements and reduced size unit cells for frequency selective surfaces," *IEE Proc. H*, Vol. 138, No. 1, 19–22, 1991.
3. Parker, E. A., A. N. A. El Sheikh, C. De, and A. C. Lima, "Convoluted frequency selective array elements derived from linear and crossed dipoles," *IEE Proc. H*, Vol. 140, No. 5, 378–380, 1993.
4. Romeu, J. and Y. Rahmit-Samii, "Fractal FSS: a novel dual band frequency selective surface," *IEEE Trans. Antennas Propagat.*, Vol. 48, No. 7, 1097–1105, 2000.
5. Bertoni, H., L. H. Cheo, and T. Tamir, "Frequency selective reflection and transmission by periodic dielectric layer," *IEEE Trans. Antennas Propagat.*, Vol. 37, No. 1, 78–83, 1989.
6. Bornemann, J., "Computer aided design of multilayered dielectric frequency selective surfaces for circularly polarized millimeter wave applications," *IEEE Trans. Antennas Propagat.*, Vol. 41, No. 11, 1588–1591, 1993.
7. Sun, L. and J. Borneman, "Design of frequency selective surfaces formed by stratified dielectric layers," *IEEE AP-S Int. Symp. Dig.*, Vol. 1, 408–411, 1992.
8. Kedar, A. and U. K. Revankar, "Parametric study of flat sandwich multilayer Radome," *Progress In Electromagnetics Research*, PIER 66, 253–265, 2006.
9. Xu, S. and Y. Li, "Frequency selective characteristics of dielectric periodic structures for millimeter wave application," *International Journal of Infrared and Millimeter Waves*, Vol. 19, No. 3, 1998.

10. Aissaoui, M., J. Zaghdoudi, M. Kanzari, and B. Rezig, "Optical properties of the quasi-periodic one-dimentional generalized multilayer Fibonacci structures," *Progress In Electromagnetics Research*, PIER 59, 69–83, 2006.
11. Tibuleac, S., R. Magnusson, T. A. Maldonado, P. P. Young, and T. R. Holzheimer, "Dielectric frequency selective structures incorporating waveguide gratings," *IEEE Trans. Microwave Theory Tech.*, Vol. 48, No. 4, 553–561, 2000.
12. Yang, H. D. and J. Wang, "Surface waves of printed antennas on planar artificial periodic dielectric structures," *IEEE Trans. Antennas Propagat.*, Vol. 49, No. 3, 444–450, 2001.
13. Yang, L. and S. Xu, "Investigation into effects of dielectric loss on frequency selective characteristics of dielectric periodic structures," *IEE Proc. H*, Vol. 148, No. 5, 302–306, 2001.
14. Coves, A., B. Gimeno, D. Camilleri, M. V. Andres, A. A. San Blas, and V. E. Boria, "Full wave analysis of dielectric frequency selective surfaces using a vectorial modal method," *IEEE Trans. Antennas Propagat.*, Vol. 52, No. 8, 2091–2099, 2004.
15. Ishimaru, A., *Electromagnetic Wave Propagation, Radiation, and Scattering*, Prentice Hall, Englewood Cliffs, 1991.
16. Kong, J. A., *Theory of Electromagnetic Waves*, Wiley Interscience, New York, 1975, 1986, 1990, EMW Publishing, Cambridge, 2000, 2005.
17. Kong, J. A., "Electromagnetic wave interaction with stratified negative isotropic media," *Progress In Electromagnetics Research*, PIER 35, 1–52, 2002.
18. Wu, T. K., *Frequency Selective Surface and Grid Array*, Wiley, New York, 1995.
19. Qing, A. and C. K. Lee, "An improved model for full wave analysis of multilayered frequency selective surface with gridded square element," *Progress In Electromagnetics Research*, PIER 30, 285–303, 2001.
20. Cory, H., S. Shiran, and M.Heilper, "An iterative method for calculating the shielding effectiveness and light Transmittance of multilayered media," *IEEE Trans. Electrogagnetic Compatibility*, Vol. 35, No. 4, 451–456, 1993.
21. Cory, H. and C. Zach, "Wave propagation in metamaterial multi layered structures," *Microwave and Optical Technology Letters*, Vol. 40, No. 6, 460–465, 2004.
22. Pendry, J. B. and A. MacKinnon, "Calculation of photon dispersion," *Phys. Rev. Lett.*, Vol. 69, No. 19, 2772–2775, 1992.

23. Pieper, R., M. Shirvaikar, and J. Salvatierra, "A transmission line model for analysis of thin film optical filters," *IEEE System Theory Symposium, USA*, 186–191, 2006.
24. Pozar, D. M., *Microwave Engineering*, Wiley, New York, 2004.
25. Gerardin, J. and A. Lakhtakia, "Negative index of refraction and distributed Bragg reflectors," *Microwave and Optical Technology Letters*, Vol. 34, No. 6, 409–411, 2002.
26. Wei, L. and J. W. Y. Lit, "Phase-shifted bragg grating filters with symmetrical structures," *Journal of Lightwave Technology*, Vol. 15, No. 8, 1997.
27. Bakhti, F. and P. Sansonetti, "Design and realization of multiple quarter-wave phase-shifts UV-written bandpass filters in optical fibers," *Journal of Llightwave Ttechnology*, Vol. 15, No. 8, 1997.
28. Vasconcelos, M. S., E. L. Albuquerque, and A. M. Mariz, "Optical spectra of a cantor superlattice," *Brazilian Journal of Physics*, Vol. 26, No. 1, 376–380, 1996.